

Statistics of grain microstructure evolution under anisotropic grain boundary energies and mobilities using threshold-dynamics

Jaekwang Kim^{a,b}, Nikhil Chandra Admal^a

^a*Department of Mechanical Science and Engineering, University of Illinois Urbana-Champaign, United States*

^b*Department of Mechanical and Design Engineering, Hongik University, Sejong, South Korea*

Abstract

This paper investigates the statistical behavior of two-dimensional grain microstructures during grain growth under anisotropic grain boundary characters. We employ the threshold-dynamics method, which allows for unparalleled computational speed, to simulate the full-field curvature motion of grain boundaries in a large polycrystal ensemble. Two sets of numerical experiments are performed to explore the effect of grain boundary anisotropy on the evolution of microstructure features. In the first experiment, we focus on abnormal grain growth and find that grain boundary anisotropy introduces a statistical preference for certain grain orientations. This leads to changes in the overall grain size distribution from the isotropic case. In the second experiment, we examine the texture development and growth of twin grain boundaries at different initial microstructures. We find that both phenomena are more pronounced when the initial microstructure has a dominant fraction of high-angle grain boundaries. Our results suggest effective grain boundary engineering strategies for improving material properties.

Keywords: grain growth, motion by curvature, grain statistics, microstructure, threshold-dynamics, polycrystalline materials, grain texture

1. Introduction

The macroscopic properties of polycrystalline materials are strongly influenced by their grain microstructure, which is determined by the thermomechanical loads during materials processing. At the macroscale, a grain microstructure is typically described by the grain boundary (GB) character distribution. GB engineering refers to the strategy of enhancing the properties of a polycrystal by transforming its GB character distribution to a target distribution using thermomechanical processes [1]. Recently, the GB engineering paradigm has been extended to tailor the properties of nanocrystalline materials, which are promising next-generation structural materials with high strength, fatigue life, and wear resistance [2, 3, 4]. For example, subjecting nanocrystalline materials to thermomechanical cycling leads to a considerable increase in the fraction of $\Sigma 3$ grain boundaries [5], which demonstrate high resistance to sliding, cavitation, and fracture [6].

Establishing the relationship between microstructure and materials properties, as well as predicting the evolution of microstructure during various manufacturing processes are ongoing research challenges in the field of GB engineering. In this regard, atomistic [7, 8, 9],

mesoscopic [10, 11], and macroscopic continuum [12, 13, 14] models have been developed over the last few decades to uncover the connection between microstructures, properties, and process parameters.

A defining characteristic of these models is the motion of GBs driven by surface tension to decrease the interfacial energy. When a polycrystalline material is annealed, grains grow to decrease the total energy of the system by reducing the GB area, leading to the motion of GBs towards their centers of curvatures. The Mullins model [15] describes such a motion as

$$v = -m\gamma\kappa, \tag{1.1}$$

where v , κ , γ , and m denote signed velocity magnitude, curvature, misorientation-dependent energy density, and mobility of the GB, respectively. If m and γ are constants, the system is called *isotropic*. Grain growth in an isotropic system is characterized by a relatively narrow range in the grain size distributions that obeys a simple scaling relation, regardless of the initial configuration of the grain microstructure [16, 17]. On the other hand, anisotropic grain growth occurs when m and γ depend on the GB character, defined by the five macroscopic degrees of freedom (dofs).¹

Recent studies have reported that microstructure evolution is heavily influenced by the anisotropy of GBs [11, 18, 19, 20]. With the aid of accurate interatomic potentials, significant progress has been made in mapping the GB anisotropy by the construction of grain boundary energies and mobilities as functions of the GB character [21, 22, 23, 24, 25]. However, precisely identifying the GB character distribution responsible for spontaneous microstructure transformation phenomena such as *abnormal grain growth* (AGG) and *recrystallization* remains a fundamental challenge in materials science. One of the main difficulties arises from the enormity of the microstructure space (relative to the space of processes and properties), which encompasses all possible configurations of grain assemblies. Due to the relatively small size of the property space, the structure-property relationship is necessarily a many-to-one mapping [26, 27]. Therefore, grain microstructures are commonly described using statistical distributions for grain sizes, topologies, and orientations, which makes it possible to express structure-property relationship using reduced order models [28, 29, 30]. For example, the reduced order model developed by Kim and Admal [28] describes the evolution of distributions for grain sizes and topologies under the idealized isotropic grain growth. Extending the model to anisotropic grain growth requires careful investigation of the role of GB anisotropy on the evolution of the statistics of a microstructure, which is the main goal of this paper.

Threshold-dynamics (TD) [31], a class of numerical methods to simulate GB motion, has proven to be highly efficient in simulating large ensembles of grains. In the TD framework, GBs are sharp interfaces that evolve according to motion by curvature, given in (1.1). Each grain is described by a level set function that is assigned a positive value within the grain and a negative value outside of it. This implies that the zero-valued isosurface of the function corresponds to the interface surrounding the grain. One advantage of the sharp interface framework is that it allows a relatively coarse grid representation of a GB compared to diffuse-interface models (including phase-field models), which require the grid to be refined

¹Here, three degrees represent a rotation associated with the misorientation between the two grains, and the remaining two degrees correspond to the inclination of the grain boundary.

enough to resolve the width of a GB. In addition, the high computational efficiency of the TD methods stems from the fast Fourier transform (FFT) algorithms used to implement the diffusion operator, which drives GB motion. In addition, the TD scheme was recently equipped with a variational structure for multi-phase settings [31]. This ensured the correct prediction of the dihedral angles between three anisotropic interfaces at triple junctions, which would necessitate considerably more computational effort to achieve using diffused-interface models [11, 32, 33]. The superior computational performance of the TD methods has enabled simulations of large collections of grains that adequately sample microstructure distributions. Martine et al. [34] used the TD method to investigate the evolution of grain size and topology distributions in two dimensions and compared them to the predictions of experiments and the phase-field-crystal method.² Peng et al. [36] examined the evolution of grain morphologies of individual grains of Ni in three dimensions and the overall grain size distribution, and compared to experiments. However, their implementation of TD was limited to an isotropic system with constant GB energy and mobility. GB anisotropy was noted as a contributing factor in instances when disagreement with experiments was identified. On the other hand, Niño and Johnson [37] implemented the TD scheme for anisotropic systems using several GB energy functions, including the energy function of Bulatov et al. [38] that depends on all five dofs of a GB. While they observed distinct signatures in the morphological evolution of individual grains for different GB energy functions, GB statistics were reported to evolve identically in all the cases. However, it must be noted that Niño and Johnson [37] assumed a unit reduced mobility, meaning that the product of the mobility and surface tension is set to one. In this case, although the dihedral angles at triple junctions are dictated by GB energy anisotropy, the anisotropy of surface tension is canceled by that of mobility. Consequently, the resulting motion by curvature remains similar to the isotropic case. In our view, it is important to isolate GB mobility to appropriately estimate the role of GB energy anisotropy. Fortunately, this is made possible by a recent update to the algorithm of Salvador and Esedoğlu [39], which allows the prescription of GB energies and mobilities independently. Using the latest TD algorithm, Salvador and Esedoğlu [40] investigated grain statistics under a constant mobility and a Read–Shockley GB energy (RSE).³ It was observed that in two dimensions, the RSE also did not lead to significant deviation in the grain size distribution compared to the isotropic case. However, since the RSE is valid for only small misorientation angles, the full extent of the impact of GB energy anisotropy on grain growth remains unexplored.

In this paper, we investigate the influence of GB anisotropy on the statistical evolution of grain microstructure and its steady state in two dimensions. Our first objective is to investigate how GB energy anisotropy affects AGG, a key feature of microstructure evolution that significantly impacts materials’ properties. Secondly, we will investigate texture development and the growth of special boundaries in initial microstructure configurations with different fractions of low-angle grain boundaries (LAGBs) and high-angle grain boundaries (HAGBs).

²The phase field crystal method resolves the atomic positions and describes their evolution at a diffusive time scale. This technique involves a free energy functional that is minimized when the density field is periodic, thereby facilitating the formation of density field patterns in solid phases [35].

³A grain boundary energy is of the Read–Shockley form, if it is a monotonously increasing concave function of the misorientation angle.

The question is particularly significant in GB engineering of nanocrystalline materials. For example, *Equal Channel Angular Pressing* (ECAP) [41, 42], which is a popular synthesizing nanostructured solids, involves severe plastic deformation of coarse-grained materials leading to substantial grain refinement and a nanostructure [43]. While it has been reported that the number of ECAP cycles largely determines the fraction of HAGB and LAGB [44], it is still not clear how these different initial microstructures evolve during subsequent annealing treatment. Our study aims to shed light on this important question.

The manuscript is organized as follows. Section 2 provides a brief introduction to the TD with anisotropic GB energy and mobility, and its implementation that ensures numerical stability. In Section 3, we present results of carefully designed numerical experiments to achieve the goals of this paper. We summarize and conclude in Section 4. Table 1 collects the abbreviations used in this paper.

| Abbreviation | Defintion |
|---------------------|---|
| GB | grain boundary |
| LAGB | low-angle grain boundary |
| HAGB | high-angle grain boundary |
| TB | twin boundary |
| HAGB* | high angle grain boundaries excluding twin boundaries |
| STGB | symmetric tilt grain boundary |
| RSE | Read-Shockley (grain boundary) energy |
| AGG | abnormal grain growth |
| TD | threshold-dynamics |
| PSP | process-(micro)structure-property |
| ECAP | equal channel angular pressing |

Table 1: List of abbreviations

2. Method

The TD algorithm employs two highly efficient operations in an alternating manner to simulate motion by curvature. The first operation is a convolution of a radially symmetric kernel with a characteristic function, which is equal to 1 inside the interface and 0 outside. In the second operation, the resulting output is subjected to point-wise *thresholding* to obtain an updated characteristic function. The TD method was originally introduced by Merriman, Bence, and Osher (MBO) [45] for a two-phase system. The key idea is that the level-set of a distance function, under the action of a diffusion operator, moves in the normal direction with a velocity equal to the mean curvature of the level-set surface. While many extensions to multi-phase systems were subsequently developed, the generalization of Esedoglu and Otto [31] demonstrates superior characteristics due to its variational structure. Moreover, recent developments to the TD method include enhanced accuracy [46], grain grouping techniques to save computational memory [47, 48], and incorporating anisotropic mobility [49]. In the following section, we summarize the TD method used in this paper.

2.1. Background

Consider a two-dimensional polycrystal $D = \cup_{j=1}^N \Sigma_j$ partitioned by N grains occupying regions Σ_j . If $\gamma_{ij}(= \gamma_{ji})$ denotes the interfacial energy density between grains Σ_i and Σ_j , the total grain boundary energy of the polycrystal is given by

$$E = \frac{1}{2} \sum_{i,j=1}^N \gamma_{ij} \text{Area}(\Gamma_{ij}), \quad (2.1)$$

where Γ_{ij} denotes the boundary between two adjacent grains Σ_i and Σ_j . If γ represents the matrix with γ_{ij} as its entries, then γ belongs to the following class of surface tension matrices

$$\mathcal{S}_N = \{\gamma \in R^{N \times N} : \gamma_{ii} = 0 \quad \text{and} \quad \gamma_{ij} = \gamma_{ji} > 0 \quad \text{for all distinct } i, j\}. \quad (2.2)$$

The steepest descent of the energy in (2.1) results in an anisotropic motion by curvature,

$$v_{ij} = -\mu_{ij} \gamma_{ij} \kappa_{ij},$$

where v_{ij} , κ_{ij} , and μ_{ij} denote the velocity, mean curvature, mobility, and mobility of the interface Γ_{ij} . The variational structure of the TD originates from the following non-local approximation of E

$$E_{\delta t}(\Sigma_1, \dots, \Sigma_N) = \frac{1}{2\delta t} \sum_{i,j=1}^N \gamma_{ij} \int_D \mathbb{I}_{\Sigma_i} K_{\delta t} * \mathbb{I}_{\Sigma_j} dx, \quad (2.3)$$

where $K_{\delta t} : \mathbb{R}^d \rightarrow \mathbb{R}$ is a positive-valued convolution kernel with a characteristic width δt , and \mathbb{I}_{Σ_i} is the characteristic function

$$\mathbb{I}_{\Sigma_i}(\mathbf{x}) = \begin{cases} 1 & \text{if } \mathbf{x} \in \Sigma_i, \\ 0 & \text{otherwise.} \end{cases}$$

Esedoğlu and Otto [31] showed that $E_{\delta t} \rightarrow E$, in the sense of Γ -convergence, as $\delta t \rightarrow 0$. $E_{\delta t}$ may be viewed as a functional of N characteristic functions. More formally, $E_{\delta t}$ is defined on the following set \mathcal{B} consisting of n -tuples of binary functions

$$\mathcal{B} = \{(u_1, \dots, u_N) : \text{for each } \mathbf{x} \in D \text{ there is an } i \text{ such that } u_i(\mathbf{x}) = 1 \\ \text{and } u_j(\mathbf{x}) = 0 \text{ for all } j \neq i\}. \quad (2.4)$$

The construction of $E_{\delta t}$ (2.3) relies on the interpretation [31] that the surface area of Γ_{ij} can be estimated by the amount of heat that escapes from Σ_i into Σ_j in δt time, i.e.,

$$\text{Area}(\Gamma_{ij}) \approx \frac{1}{\delta t} \sum_{i,j=1}^N \int_D \mathbb{I}_{\Sigma_i} K_{\delta t} * \mathbb{I}_{\Sigma_j} dx. \quad (2.5)$$

While a common choice of $K_{\delta t}$ is the Gaussian kernel

$$G_{\delta t}(\mathbf{x}) = \frac{1}{(4\pi\delta t)^{\frac{d}{2}}} \exp\left(-\frac{|\mathbf{x}|^2}{4\delta t}\right), \quad (2.6)$$

alternate kernels have been proposed more recently.

A point-wise thresholding rule is designed to move grain boundaries in their normal direction by distances of $\gamma_{ij}\mu_{ij}\kappa_{ij}\delta t$ at every time step, such that the energy $E_{\delta t}$ monotonically decreases. The characteristic width, δt , of the kernel corresponds to the time step size t_S . The parameter δt also determines the minimum grid size $\delta x < \gamma_{ij}\mu_{ij}\kappa_{\min}\delta t$ required by the TD algorithm, where κ_{\min} is the minimum curvature (such as the curvature of the largest grain in D). If the grid size condition is not satisfied, grain boundaries would stagnate. The variational nature of the TD algorithms ensures the correct equilibrium dihedral angle condition at triple junctions (known as Herring angle condition [50]) is satisfied [31].

2.2. Algorithm

The TD scheme employed in this paper is a recent version proposed by Salvador and Esedoğlu [39]. Comparing to the original version [31], the current TD scheme broadens the choice of anisotropic mobilities μ_{ij} with minimum algorithmic complication. This is achieved by constructing the kernel $K_{\delta t}$ using two Gaussian kernels with distinct non-negative width parameters α and β as

$$K_{\delta t} = a_{ij}G_{\sqrt{\alpha\delta t}} + b_{ij}G_{\sqrt{\beta\delta t}}, \quad (2.7)$$

where

$$a_{ij} = \frac{\sqrt{\pi\alpha}}{\alpha - \beta}(\gamma_{ij} - \beta\mu_{ij}^{-1}), \quad (2.8)$$

and

$$b_{ij} = \frac{\sqrt{\pi\beta}}{\alpha - \beta}(-\gamma_{ij} + \alpha\mu_{ij}^{-1}). \quad (2.9)$$

The evolution of grain domains $\Sigma_1^n, \dots, \Sigma_N^n$ at the n -th step involves three steps. First, convolutions $\phi_{1,i}^n := G_{\sqrt{\alpha\delta t}} * \mathbb{I}_{\Sigma_i^n}$ and $\phi_{2,i}^n := G_{\sqrt{\beta\delta t}} * \mathbb{I}_{\Sigma_i^n}$ are computed. Second, comparison functions $\psi_i^n := \sum_{i \neq j} a_{ij}\phi_{1,j}^n + b_{ij}\phi_{2,j}^n$ are assembled. In the final step, thresholding is carried out using the criterion

$$\Sigma_i^{n+1} = \{\mathbf{x} : \psi_i^n(\mathbf{x}) < \min_{j \neq i} \psi_j^n(\mathbf{x})\}. \quad (2.10)$$

The aforementioned steps are summarized in Algorithm 1.

In real materials, the dependence of GB energies and mobilities on the misorientation is highly complex with multiple local maxima/minima. However, Algorithm 1 and other TD versions are restricted to the following class of GB energies

$$\mathcal{T}_N = \{\gamma \in \mathcal{S}_N : \gamma_{ij} + \gamma_{jk} \leq \gamma_{ik} \text{ for any } i, j, k\}, \quad (2.11)$$

which includes energies that satisfy a triangle inequality. If $\gamma \notin \mathcal{T}_N$, a TD scheme may lead to grain boundary wetting by nucleating a new grain along one of the existing boundaries [31]. Such a nucleation is entirely a numerical artifact and thus unphysical. Wetting can be circumvented by restricting the thresholding condition in (2.10) to j in the neighborhood of

i. In addition, for the TD algorithm to be numerically stable — i.e., dissipate E at every iteration regardless of the choice of δt — the surface tension matrix has to be *conditionally negative semi-definite*, which implies $\gamma \in \mathcal{S}_N$ has to satisfy ⁴

$$\sum_{i,j}^N \gamma_{ij} \xi_i \xi_j \leq 0 \quad \text{whenever} \quad \sum_i^N \xi_i = 0. \quad (2.12)$$

If condition (2.12) fails, the algorithm could lead to erroneous movement of a grain boundary network; possibly, the TD algorithm causes the local energy of the system to increase, despite the overall free energy decreasing. While Esedoğlu and Otto [31] proved that the stability condition (2.12) is satisfied for energies sampled from the RSE form regardless of the size N of the system, the stability condition may not hold for general GB energy functions.

In addition, Algorithm 1 also requires the matrix of reciprocal mobilities $1/\mu$, with entries μ_{ij}^{-1} , to be conditionally negative semi-definite. If γ and $1/\mu$ are conditionally negative-semidefinite, a judicious choice of parameters α and β will ensure the unconditional stability of the algorithm. In Ref. [39], it was shown that

$$\alpha \geq \frac{\min_{i=1,\dots,N-1} s_i}{\max_{i=1,\dots,N-1} m_i} \quad \text{and} \quad \beta \leq \frac{\max_{i=1,\dots,N-1} s_i}{\min_{i=1,\dots,N-1} m_i} \quad (2.13)$$

guarantees unconditional stability. In (2.13), s_i and m_i are the nonzero eigenvalues of matrices $J\gamma J$ and $J\frac{1}{\mu}J$, where $J = I - \frac{1}{N}\mathbf{e} \otimes \mathbf{e}$ and $\mathbf{e} = (1, \dots, 1)$. Note that α and β that satisfy (2.13) automatically guarantee the positiveness of the kernel ($K > 0$), which is an essential condition for TD algorithms to attain the viscosity solution for corresponding interfacial motion [51].

3. Simulations

We will now present a statistical study of grain microstructure evolution under anisotropy energies and mobilities in large two-dimensional polycrystals using Algorithm 1. In particular, we focus on the following two phenomena:

1. Onset of AGG under anisotropic grain boundary energy and mobility
2. Development of texture during grain growth

3.1. Abnormal grain growth

AGG refers to the enlargement of a minority of grains in a polycrystal at the expense of the surrounding grains [52], and is widely observed in many systems including thin films. AGG contrasts with normal grain growth, characterized by a relatively narrow grain size range and a self-similar grain size distribution in time [53]. While anisotropy in GB properties has been proposed as the underlying cause of AGG [54], quantitatively validating the hypothesis is a challenging task due to the complexity of GB anisotropy, expressed as a function of five

⁴Condition (2.12) implies γ is a matrix that is negative semi-definite as a quadratic form on $(1, \dots, 1)^\perp$.

Algorithm 1 Threshold-dynamics of Salvador and Esedog̃lu [39]

Input: The surface tension matrix γ , the mobility matrix μ , the initial grain structure $\Sigma_1^0, \dots, \Sigma_N^0$ described on a discrete grid of which size is δx , and the final time T

Output: Σ_N^{n+1} at the $(n+1)$ -th time from the grain shapes $\Sigma_1^n, \dots, \Sigma_N^n$

1: Choose the kernel width δt (equivalent to the time step size t_s of the algorithm) ensuring:

$$\delta x < \gamma_{ij} \mu_{ij} \kappa_{\min} \delta t$$

2: Choose α and β according to (2.13)

3: Construct the two Gaussians $G_{\sqrt{\alpha\delta t}}$ and $G_{\sqrt{\beta\delta t}}$

4: $t = 0$

5: **while** $t < T$ **do**

6: Compute the convolutions:

$$\phi_{1,i}^n = G_{\sqrt{\alpha\delta t}} * \mathbb{I}_{\Sigma_i^n} \quad \text{and} \quad \phi_{2,i}^n = G_{\sqrt{\beta\delta t}} * \mathbb{I}_{\Sigma_i^n}$$

7: Form the comparison functions:

$$\psi_i^n = \sum_{i \neq j} a_{ij} \phi_{1,j}^n + b_{ij} \phi_{2,j}^n$$

where a_{ij} and b_{ij} are given by (2.8) and (2.9)

8: Update the grain shapes:

$$\Sigma_i^{n+1} = \{\mathbf{x} : \psi_i^n(\mathbf{x}) < \min_{j \neq i} \psi_j^n(\mathbf{x})\}$$

9: $t = t + t_s$

10: **end while**

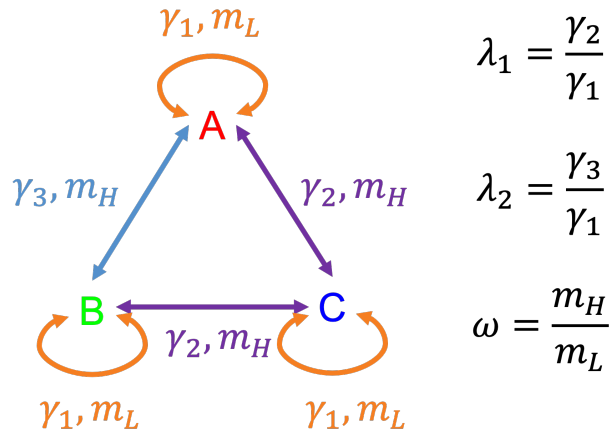


Figure 1: A mnemonic depicting grain boundary anisotropy of a polycrystal used to study AGG in Section 3.1.

dofs of the grain boundary character. Moreover, there is no agreement on which particular microstructural characteristics signify the existence of AGG [52]. This motivates a statistical study on AGG in a simplified system amenable for further analysis.

3.1.1. AGG in an anisotropic tricrystal

To investigate and analyze AGG, we considered a polycrystal with grains belonging to three distinct groups (A, B, and C), and described by a few parameters. Due to its simplicity, this system serves as a minimal example that leads to AGG. We assume that the misorientations between grains within each group are small and the GBs formed by them have identical energies. On the other hand, it is assumed that grains belonging to different groups are highly misoriented and the GB energies between them are larger than the energy of those formed between grains from the same group. If γ_{ij} ($i = A, B$ or C) denotes the GB energy between the i -th and the j -th groups of grains, then we have $\gamma_{AA} = \gamma_{BB} = \gamma_{CC} := \gamma_1$ and γ_{AB} , γ_{BC} , and γ_{CA} are greater than γ_1 . In addition, we also assume that $\gamma_{CA} = \gamma_{BC} := \gamma_2$ is smaller than $\gamma_3 := \gamma_{AB}$. This implies the orientation angles of grains in group C are closer to those in A and B than A -grains are to B -grains. We also assume the system has only two mobilities — one for small misorientation angle GBs m_L (for the same group) and the other for larger misorientation angles m_H (for different groups).

The aforementioned GB anisotropy is characterized by three non-dimensional parameters — $\lambda_1 = \gamma_2/\gamma_1$ and $\lambda_2 = \gamma_3/\gamma_1$ describe energy anisotropy, and $\omega = m_H/m_L$ describes the anisotropy in mobility. Note that if all the parameters are equal to one, the system is isotropic. The mnemonic in Fig. 1 depicts the GB anisotropy of our system. We investigated the following three cases:

1. Case 1a: isotropic grain growth, i.e., $\lambda_1 = \lambda_2 = 1.0$ and $\omega = 1.0$
2. Case 1b: energy ratios $\lambda_1 = 1.5$ and $\lambda_2 = 2.0$, and mobility ratio $\omega = 1.0$
3. Case 1c: energy ratios $\lambda_1 = 1.5$ and $\lambda_2 = 2.0$, and mobility ratio $\omega = 1.2$

In Case 1b and 1c, the strengths of GB anisotropy parameters remain *weak* so that γ

satisfies the stability condition (2.12) of the Algorithm 1.⁵ However, in these cases, C-type grains are still energetically favored and we anticipate unusual growth of C-type growth.

In all of the cases, we begin with the initial grain microstructure configuration, shown in Fig. 2a. The initial microstructure consists of a total of 8,000 grains generated from the Voronoi tessellations of uniformly distributed random points in the region $\Omega = [0, 1]^2$, discretized by a 3000×3000 regular grid. Each grain is randomly assigned to one of three groups from A to C, such that the number fractions and the area fractions of the three groups are equal to 1/3. In Fig. 2a, the red (group A), green (group B), and blue (group C) colors distinguish the three groups.

3.1.2. Results

Simulations are carried out with a time step size $t_S = 5.57 \times 10^{-7}t$ where t is a unit conversion factor with dimension $[\text{time}][\text{length}]^{-2}$. Grain microstructures at time $t_1 = 2.78 \times 10^{-4}t = 500t_S$ for the three cases are shown in Fig. 2b-Fig. 2d. At the end of the simulations, microstructures of cases 1a, 1b, and 1c contain 2563, 1984, and 1797 grains, respectively. This implies GB anisotropy increases the rate of grain coarsening. Comparing Fig. 2b to Fig. 2c and Fig. 2d, we observe that anisotropy results in clustering of grains belonging to the same groups and an increase in the area fraction of C-type grains.

Next, we examine and compare the statistical features of the microstructure evolution in the three cases. Fig. 3a shows plots of grain size distributions at $t = t_1$. The x -axes represent grain areas normalized by the average grain area at $t = t_1$, and the y -axes represents the probability density, which implies the areas under the graphs are equal to one. To compute the probability density, a bin size of 0.1 was used to partition the x -axes. From Fig. 3a, we conclude that the three grain size distributions are similar for most of the normalized grain areas. However, comparing the distributions is a delicate exercise as abnormally grown grains are spatially rare [52], and therefore, AGG manifests in the tail of a distribution. A closeup of the tails (yellow shaded region in Fig. 3a) of the distributions is shown in Fig. 3b, which clearly shows that abnormally larger grains ($A/A_{\text{avg}} \geq 3.5$) are observed only in cases 1b and 1c.

To further investigate the role of each grain type, grain size distribution of each group is separately plotted in Fig. 4. Similar to Fig. 3, x -axes represents normalized grain sizes. However, the y -axes represent densities (number fractions) calculated for individual groups. While the distributions of grain types are identical in the isotropic case (Fig. 4a), the C-type grain has an extended tail and a smaller peak value in the presence of anisotropy in cases 1b and 1c (Fig. 4b and Fig. 4c). In other words, anisotropy results in the abnormal growth of C-type grains and lower (relative to the isotropic case) number of smaller grains. The latter is not only a consequence of AGG but also grain shrinkage, which can be reasoned as follows. If a C-type grain is surrounded by grains of similar type but not C-type, it is energetically favorable for it to shrink as $\gamma_1 < \gamma_2$. On the other hand, if a C-type grain is surrounded by grains of different types (A or B), growth is preferred since $\gamma_2 < \gamma_3$.

Table 2 lists the number fraction and areas of grains of different types measured in the three case studies. The number fraction and the area of C-type grains is the maximum in

⁵In Ref. [31], it is provided that a necessary condition for satisfying (2.12) is that the matrix $\sqrt{\gamma}$ belongs to \mathcal{T}_N .

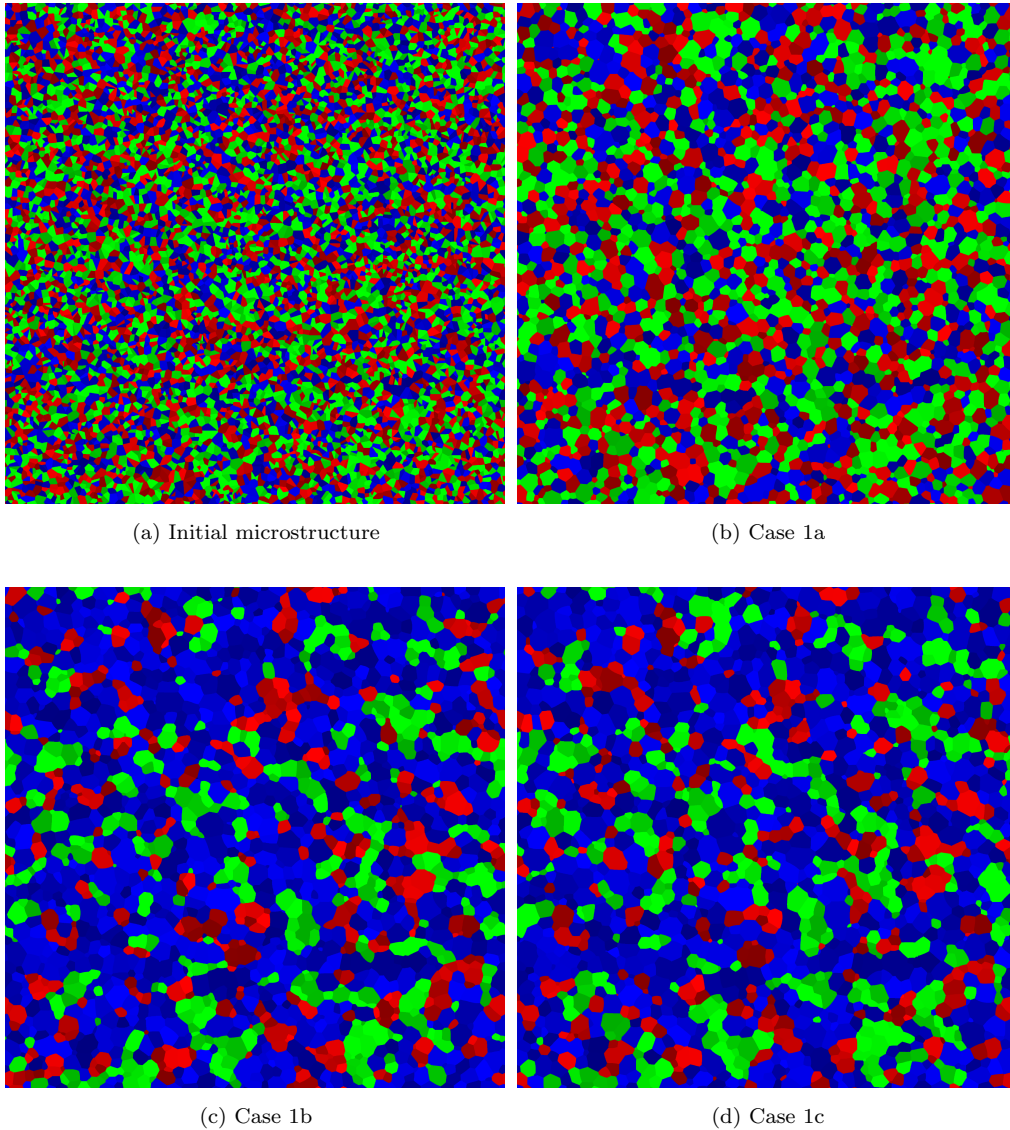


Figure 2: Grain microstructure at time $t_1 = 500t_s$ for the cases summarized in Section 3.1. The initial microstructure (a) contains 8,000 grains. The numbers of remaining grains in (b), (c), and (d) are 2563, 1984, and 1797, respectively, implying GB anisotropy increases the rate of grain coarsening.

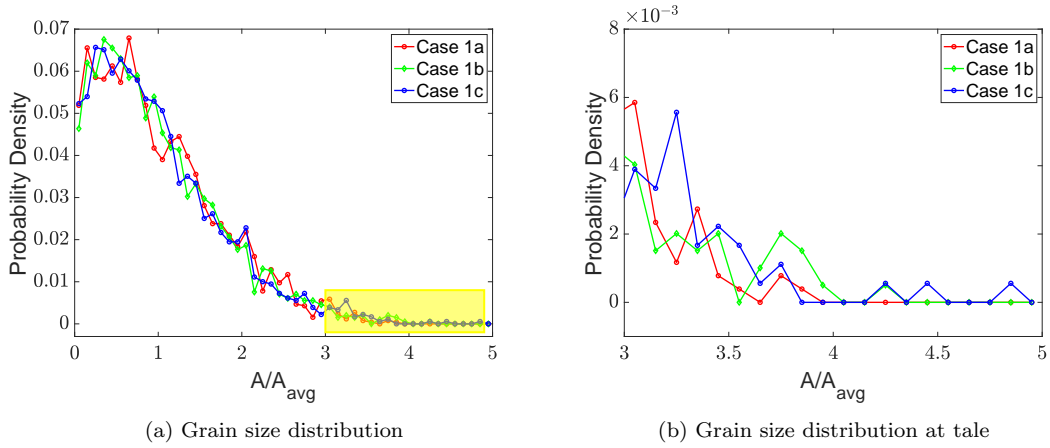


Figure 3: Grain size distributions of the cases considered in Section 3.1. A closeup of the tail region, depicted in yellow shade in (a), shows that abnormally larger grains ($A/A_{\text{avg}} \geq 3.5$) are only observed in Case 1b and Case 1c.

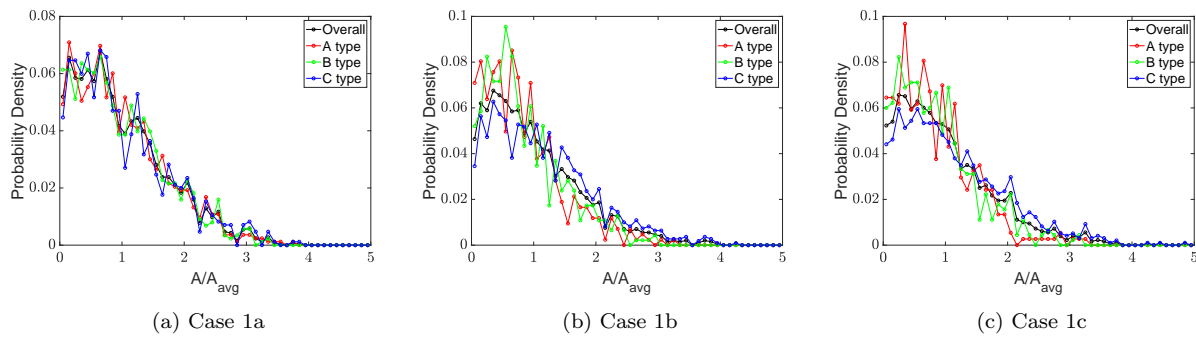


Figure 4: Grain size distributions of each group of grains for the three cases introduced in Section 3.1. The results of anisotropic case (b, c) show that the C groups are statistically preferred in Case 1b and Case 1c, resulting in a distinguished grain size distribution from the overall size distribution.

| | | A | B | C |
|---------|-----------------|--------|--------|--------|
| Case 1a | Number Fraction | 0.3246 | 0.3433 | 0.3320 |
| | Area Sum | 0.3236 | 0.3383 | 0.3381 |
| Case 1b | Number Fraction | 0.2070 | 0.2504 | 0.5426 |
| | Area Sum | 0.1730 | 0.2143 | 0.6127 |
| Case 1c | Number Fraction | 0.2132 | 0.2324 | 0.5544 |
| | Area Sum | 0.1739 | 0.1957 | 0.6304 |

Table 2: The number and area fractions of each group at time $t_1 = 500t_s$ for Case 1a to 1c.

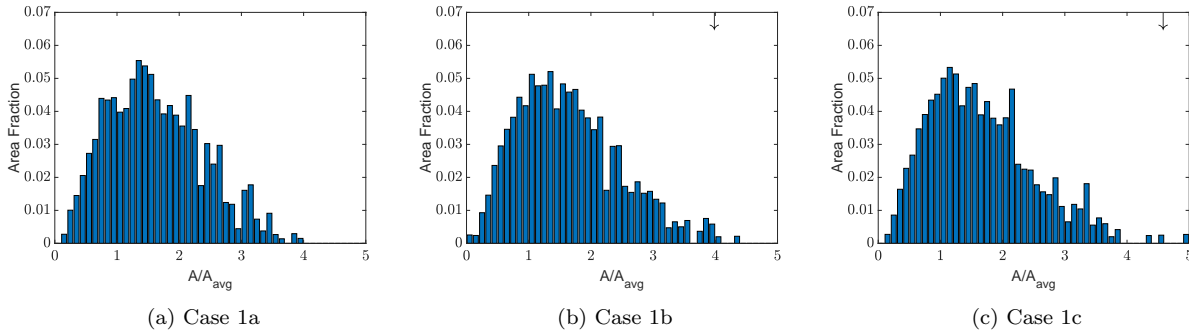


Figure 5: Grain size distribution in terms of area fractions. The same bins are used as Fig. 3. The grain boundary energy anisotropy (b) triggers a bimodal distribution, while anisotropy mobility (c) moves the location of the second mode further right.

Case 1c. This quantitative comparison shows that mobility anisotropy (Case 1c) enhances the effects of energy anisotropy (Case 1b).

Fig. 5 shows plots of *area fractions* versus the normalized grain sizes for the three cases. Compared to the probability density plots (Fig. 3 and Fig. 4), AGG is more conspicuous in the area fraction plots as the smaller number of large-sized grains have a significant effect in the latter plots. In Fig. 5b, we observe that GB energy anisotropy triggers a bimodal distribution, as predicted by a mean-field theory of Abbruzzese and Lücke [55]. In the presence of anisotropic grain boundary mobilities (Case 1c), Fig. 5c shows that the second mode moves further right.

In summary, GB anisotropy introduces a *statistical preference* to grains with particular orientations, resulting in inhomogeneity in grain size distributions and spatial arrangements. As the strength of anisotropy increases, it will eventually lead to abnormal grain growth as seen in experiments [52].

3.2. Texture formation

In this section, we study the role of grain boundary anisotropy and bicrystallography on the process of texture formation during grain growth. For this study, we consider atomistically informed grain boundary energies that respect the boundary's bicrystallography. For example, Fig. 6 shows a plot of energy versus misorientation angle for a [110]

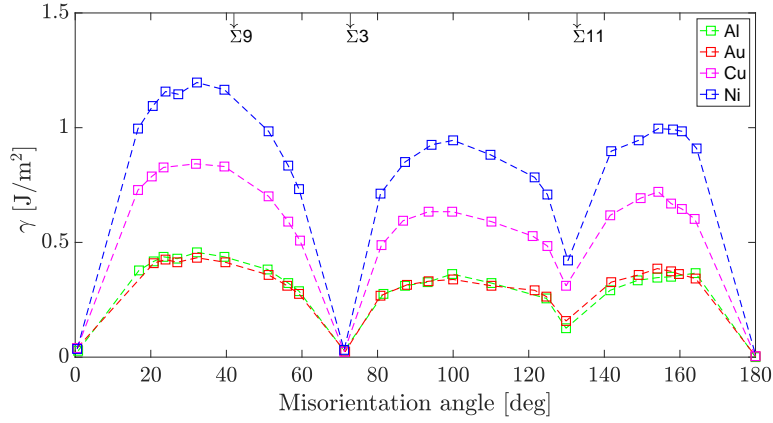


Figure 6: Molecular dynamics predictions on grain boundary energy density as a function of misorientation angle for a [110] symmetric-tilt grain boundary in face-centered-cubic materials [56, 57]. Misorientations corresponding to low energy Σ boundaries are marked on the upper axis.

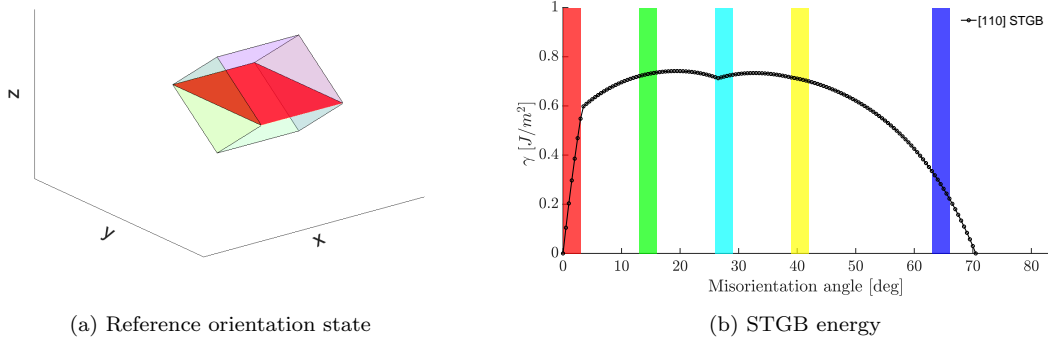


Figure 7: The [110]-STGB grain boundary energy up to misorientation angle 70.6° from the reference state shown in (a). The sub-domains for group A to E, in which grain orientations are sampled, are colorized in (b).

symmetric tilt grain boundary energy (STGB).⁶ The plot shows characteristic local minima, marked as $\Sigma 3$ and $\Sigma 11$, due to enhanced lattice matching of the grains [22, 58] at certain misorientation angles. In the following section, we describe the polycrystal and the bicrystallography respecting grain boundary energy function used to explore texture formation.

3.2.1. The system

We consider a two-dimensional fcc polycrystal with the $\langle 110 \rangle$ direction of all grains aligned along the z -axis. All grain boundaries are assumed to be $[110]$ symmetric-tilt type. The orientations of the grains are measured with respect to a reference grain whose $[100]$ direction is aligned along the x -axis, as depicted in Fig. 7a. Under these constraints, we only need a single scalar θ_i to describe the orientations of grain samples.

To strategically investigate the roles of low and high-angle grain boundaries, we restricted the grain orientations, θ_i , to groups of 3° -length intervals of the misorientation angle as follows:

$$\theta_i \in \begin{cases} \text{Group A, if } \theta_i \in [0, 3]^\circ, \\ \text{Group B, if } \theta_i \in [13, 16]^\circ, \\ \text{Group C, if } \theta_i \in [26, 29]^\circ, \\ \text{Group D, if } \theta_i \in [39, 42]^\circ, \\ \text{Group E, if } \theta_i \in [63, 66]^\circ. \end{cases} \quad (3.1)$$

The above intervals are shown in color in Fig. 7b. Boundaries between grains from the same group are identified as LAGBs with misorientation $< 3^\circ$. HAGBs of the system are formed by grains from different groups, and have a misorientation angle $> 10^\circ$. Groups A and E in (3.1) are constructed such that the misorientation of a grain boundary between an A-type grain and an E-type grain is close to that of a twin boundary (TB), which has a misorientation angle of 70.6° . TBs are often desired in grain boundary engineering as they enhance the strength and ductility of a polycrystal [59, 60]. The energies of LAGBs are typically lower than those of HAGBs and increase steeply with misorientation angles (Fig. 7b). The energy of a typical HAGB is less sensitive to changes in the misorientation angle. However, TBs are HAGBs that are exceptions to the above two properties as can be inferred from Fig. 7b.

In this study, we explored microstructures *with* and *without* subgrains. In the latter, grains are partitioned into subgrains, which are connected along LAGBs. Subgrains are commonly observed in polycrystalline materials subjected to plastic deformation followed by *recovery* at a temperature below the recrystallization temperature. The mechanism is as follows. Plastic deformation leads to an increase in dislocations, which subsequently rearrange during the recovery process to form LAGBs and subgrains. Further deformation promotes the rotation of subgrains resulting in the transformation of LAGBs into HAGBs [61, 62]. Recent progress in *severe plastic deformation*, employed during manufacturing processes, can be used to facilitate this mechanism [43, 44].

The following initial microstructures are considered in our simulations:

1. Case 2a: a tricrystal with subgrains, wherein the three primary grains belong to A, B,

⁶The domain of the plot in Fig. 6 is restricted to misorientation angles up to 180° since γ is symmetric about 180° misorientation angle due to the lattice symmetry.

| | Number of subgrains | Number of grains | Grid size | Time step t_S |
|---------|---------------------|------------------|--------------------|-----------------------|
| Case 2a | 5000 | 3 | 3000×3000 | 4.44×10^{-6} |
| Case 2b | 5000 | 30 | 3000×3000 | 2.22×10^{-6} |
| Case 2c | - | 5000 | 3000×3000 | 2.22×10^{-6} |

Table 3: Microstructure and simulation parameters of numerical experiments considered in Section 3.2

and D groups. TBs are excluded

2. Case 2b: a polycrystal with subgrains. TBs are included, and LAGBs are dominant.
3. Case 2c: a polycrystal without subgrains. TBs are included, and HAGBs are dominant.

In all cases, we examine 5,000 distinct subgrains (or only grains for Case 2c) arranged in a periodic domain discretized by a regular grid of size 3000×3000 . The mobility ratio between high to low angle grain boundary is again set to $\omega = 1.2$.

The initial tricrystal microstructure of Case 2a is shown in Fig. 8a, wherein grains and subgrains are colored based on the color keys (Fig. 7b) of the groups they belong to. The tricrystal consists of A (red), B (green), and D (yellow) type grains. The subgrains have the same color as the grain they belong to and are shaded depending on their orientation relative to their parent grain. By construction, boundaries between different colored grains are HAGBs. The microstructure was generated using a Voronoi tessellation of random seeds. Orientation groups are determined by the location of Voronoi seeds, while specific orientation values are randomly chosen within the domain of each group.

Cases 2b and 2c are designed to evaluate the role of TBs. The initial microstructure for Case 2b is shown in Fig. 9a, wherein the TBs are the boundaries between type A (red) and type E (blue) grains. It was generated using a two-level Voronoi tessellation [63]. The coarse-level Voronoi seeds are used to determine group types, while the $30\times$ -refined seeds define specific orientation values. This procedure yields a LAGB-dominated polycrystal wherein each grain is comprised of approximately 160 subgrains. On the other hand, The microstructure of Case 2c generated from a single-level Voronoi tessellation is dominated by HAGB. The initial microstructures of cases 2b and 2c, however different, have similar uniform grain orientation distributions (Fig. 10a and Fig. 12a), and therefore, are non-textured. Table 3 documents the microstructure and simulation parameters of the three case studies of this section.

An implementation of Algorithm 1 for a large-sized system is a delicate exercise. Typically, a moderate quotient α/β of the widths of the two Gaussians (2.7) is chosen so that the two Gaussians, $G_{\sqrt{\alpha\delta t}}$ and $G_{\sqrt{\beta\delta t}}$, are well-resolved even at a fairly refined grid [39]. In a large-scale system with a wide range of grain boundary energies, however, a naive choice of the width parameters (2.13) easily becomes ill-posed, because the minimum grain boundary energy in the system can be arbitrarily small. To address the issue, we follow the suggestion in Ref. [39]. The idea is to limit the possible minimum misorientation angles between any two grains to no more than 0.5° when constructing the two Gaussian kernels. This is equivalent to setting the minimum energies that can be resolved by the algorithm.

3.2.2. Results

Case 2a:

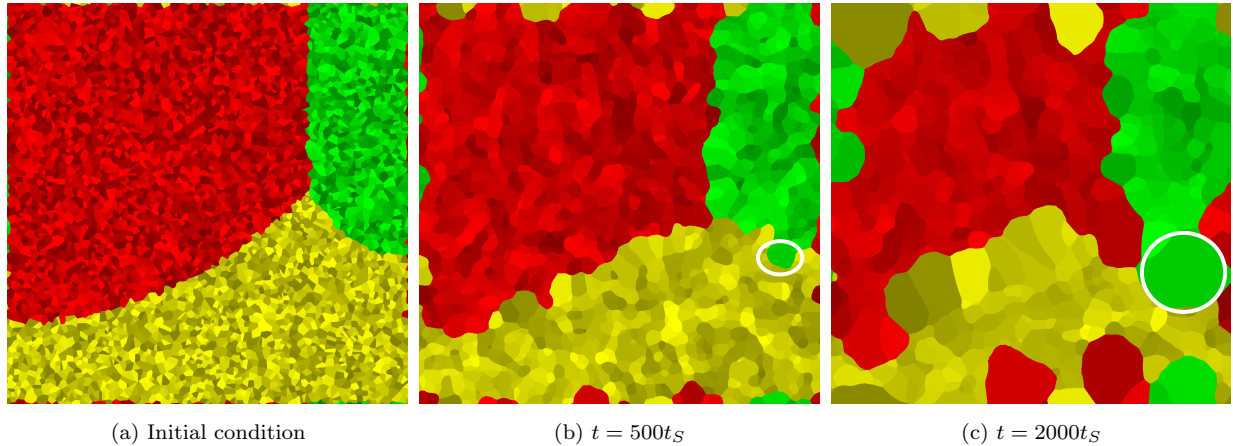


Figure 8: Microstructure evolution of a tricrystal consisting of subgrains (same colored grains). The white circled subgrain is an example of abnormally growing grain near grain boundaries.

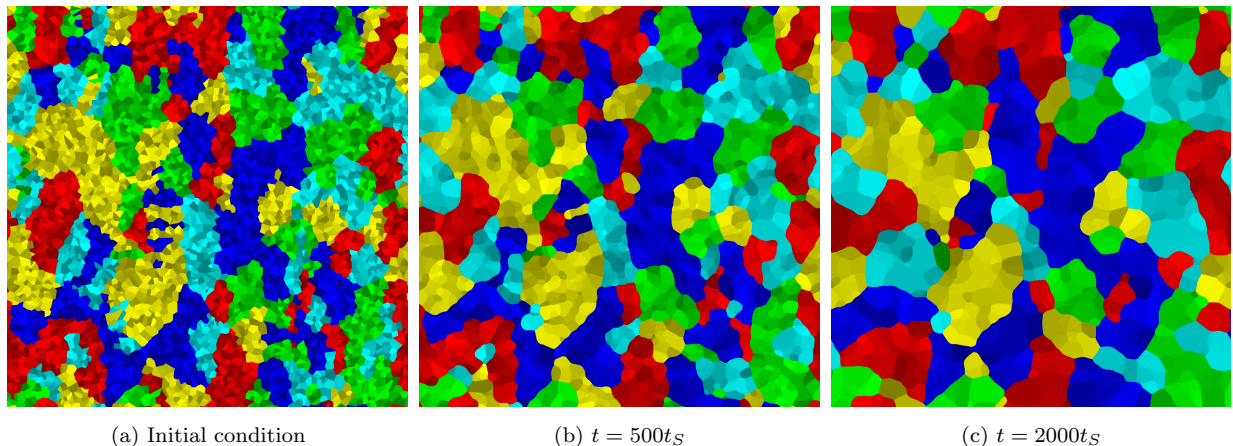


Figure 9: Microstructure evolution of a polycrystal consisting of subgrains (same colored grains). The boundaries between groups A (red) and E (blue) are twin grain boundaries.

Fig. 8a through Fig. 8c show the time evolution of the tricrystal with subgrains. All subgrains in the initial microstructure have comparable sizes. From Fig. 8b, we can infer that the grain coarsening rate is higher near a HAGB because of the higher energy and mobility of a HAGB. Fig. 8b and Fig. 8c shows that when a grain (circled) near a HAGB reaches a critical size, it undergoes AGG. It is important to note that the critical size plays an important role in selecting grains as not all grains near HAGBs undergo AGG. A plausible explanation for this observation is that beyond a critical size, it is energetically favorable for the subgrain to grow in size and absorb the subgrain boundaries in the adjoining grain. The critical size may depend on the relative sizes of the grains compared to neighbors. As a result, certain subgrains located close to grain boundaries are more likely to outgrow those located in the interior, as shown in Fig. 8c. It is interesting to note that this mechanism resembles *discontinuous recrystallization*, wherein new defect-free grains nucleate near HAGBs and grow to replace the microstructure entirely.

Fig. 9a through Fig. 9c show the time evolution of a grain microstructure with subgrains and a high fraction of LAGBs. Similar to Case 2a, certain subgrains located close to a

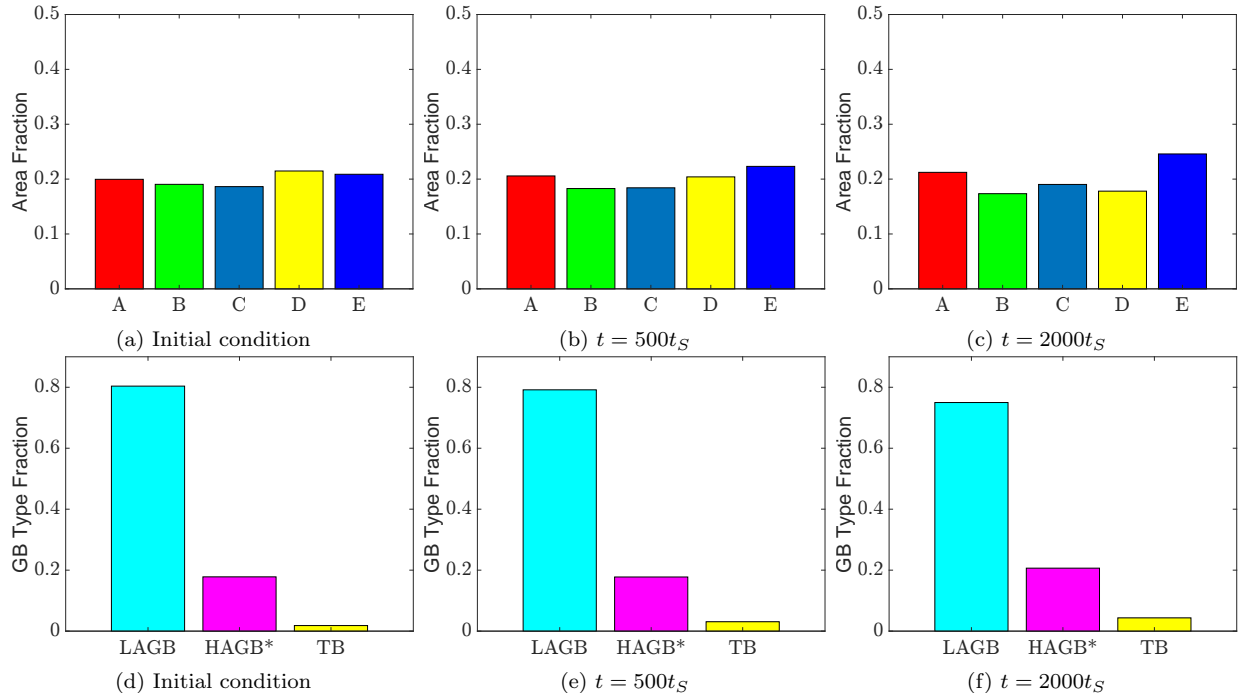


Figure 10: Texture (b-c) and types of grain boundary (e-f) changes during grain growth of a LAGB dominant polycrystal. HAGB* refers high-angle grain boundaries excluding TBs.

GB begin to grow at the expense of subgrains of the adjoining grain. To examine how the statistics of the microstructure evolve, we classified the grains into three types: LAGB, HAGB*, and TB, where HAGB* represents high-angle grain boundaries that are not TBs. Fig. 10a to Fig. 10c show plots of the area fraction of each group (A to E) and Fig. 10d to Fig. 10f show the fraction of GB types, at three different times. The plot in Fig. 10d shows that the majority of GBs in the initial microstructure are LAGBs, and only a negligible fraction of them are TBs. Since TBs have low energy, we expect area fractions of grain types A and E — which together form a TB — to grow. However, we observe that there is only a marginal increase in their area fractions in the final microstructure (Fig. 10c). The increase in the fraction of TBs is also negligible. Based on the above observation, we conclude that in a system with a high fraction of LAGBs, there is no strong preference for TBs and texture does not form.

Next, we examine the microstructure evolution in Case 2c wherein HAGBs are dominant and the system has no subgrains. Expectedly, the initial microstructure shown in Fig. 11a has no subgrains. The initial fraction of TB is also higher than Case 2b (Fig. 12d). However, the initial texture, seen in Fig. 12a, is not as strong as previous. In this case, as grain growth continues, grains from the same groups coalesce (Fig. 11b), because the system penalizes HAGB*, which have higher energies. During this process, the fractions of both LAGB and TBs steeply increase at the expense of HAGB*. Consequently, the final microstructure (Fig. 11c) shows a considerable growth of type A and E grains, indicating texture development in the microstructure. In Fig. 12f, we also observed that the growth of TBs is substantially facilitated using an initial microstructure with a high fraction of HAGB.

Lastly, we discuss the results of the present simulations in comparison to recent exper-

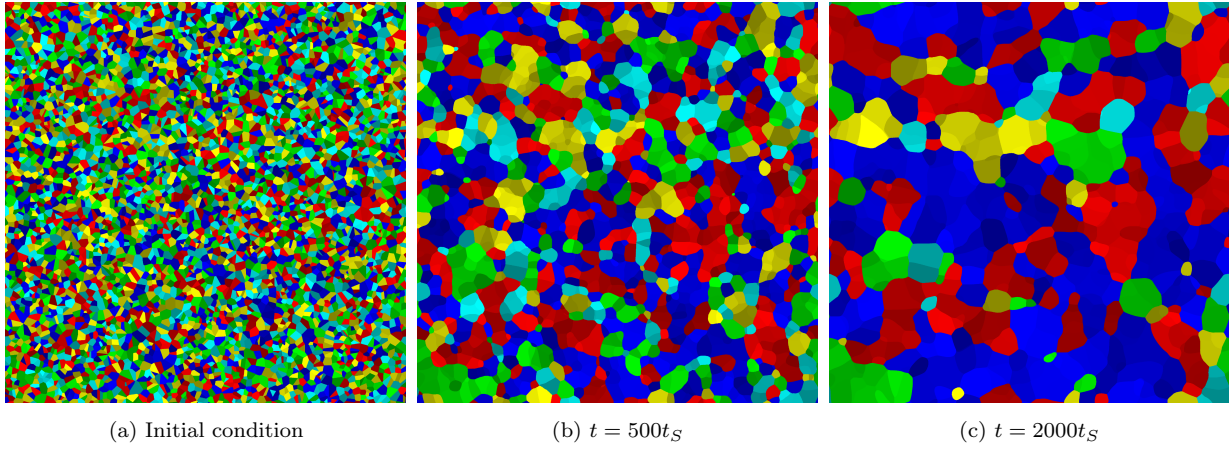


Figure 11: Microstructure evolution of a HAGB dominant polycrystal (a). The boundaries between groups A (red) and E (blue) are twin grain boundaries. Grains from the same group coalesce first (b) and type A and E grains become dominant (c).

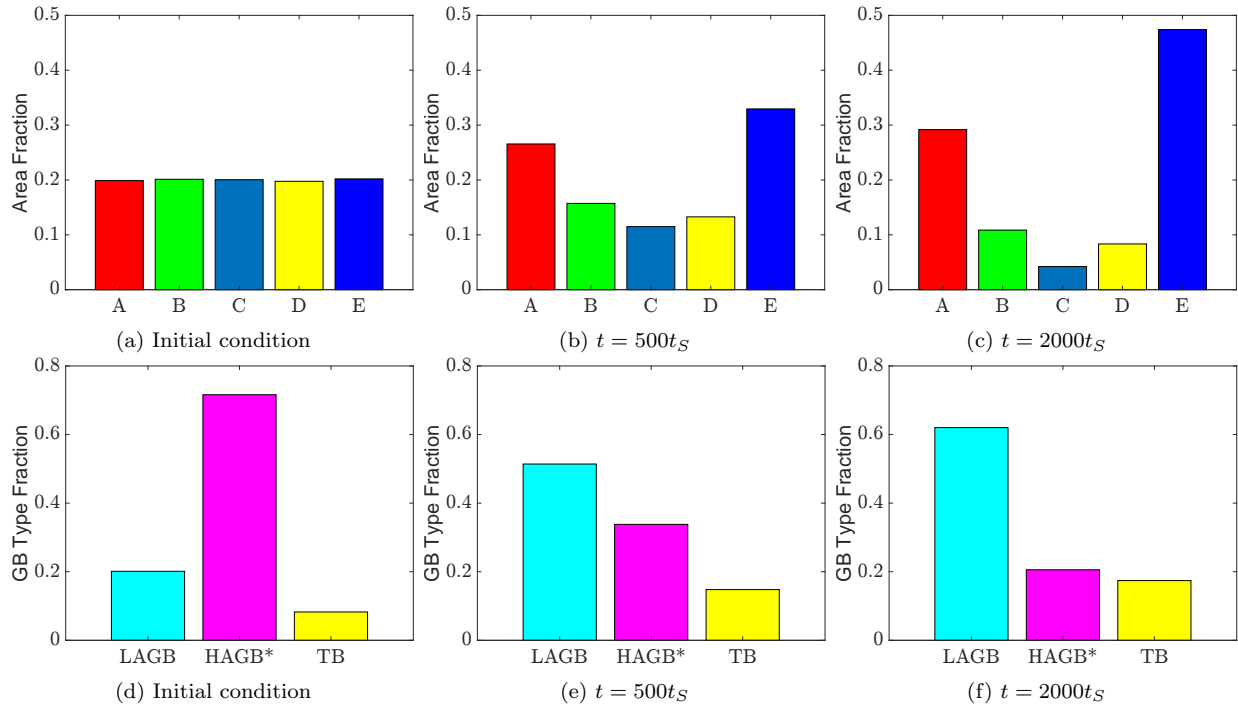


Figure 12: Texture (b-c) and types of grain boundary (e-f) changes during grain growth of a HAGB dominant polycrystal. HAGB* refers to high-angle grain boundaries excluding TBs.

imental observations of TB development in nanocrystalline materials [64]. Julie et al. [64] investigated the effect of grain size on texture formation during annealing using electrodeposited nickel samples with different average grain sizes, ranging from 20 nm to 200 nm. It is observed that the fraction of TBs in the final microstructure increases as the average grain size in the initial microstructure decreases. This trend is attributed to the relationship between the probability of accidental twin formation and the velocity of the migrating grain boundary, which in turn is inversely proportional to grain size. In our simulation, the initial microstructure of Case 2c can also be viewed as a substantially smaller average grain size than that of Case 2b (if one ignores its sub-microstructure). Since smaller grains coarsen faster, the grains in Case 2c have a higher probability of forming new grain boundaries during the same period of time, which also increases the probability of forming twin grain boundaries. In this regard, our simulation results of Case 2c are consistent with experimental observations. Yet, it is also important to note that the size difference is not the only factor in our simulations. The main difference between cases 2b and 2c is the fraction of grain boundary types in the initial condition. Unfortunately, however, since the initial fractions of GB types are not reported in Ref. [64], a conclusive discussion cannot be made at this time.

4. Conclusion

A fundamental open problem in materials science is to establish the relationship between process parameters and the evolution of grain microstructure. Given that the process-structure relationship is inherently statistical, it is necessary to use lightweight models that can efficiently capture the microstructure evolution of a polycrystal ensemble. Recent years have seen considerable advances in threshold-dynamics techniques, which have revolutionized the way to simulate full-field grain microstructure evolution during growth. The method serves as a highly efficient and robust algorithm for statistical studies on grain microstructure.

In this paper, we utilized the TD method to investigate the statistical behavior of grain microstructure under anisotropic GB characters, with a focus on abnormal grain growth and texture development. To ensure the numerical stability of the algorithm and reliable result dynamic evolution of the grain network, we imposed a restriction on the degree of GB anisotropy. We considered GBs with energies and mobilities that are compatible with the fundamental restrictions of the threshold-dynamics method.

Our first numerical experiment involves a system with the simplest GB anisotropy, which facilitates the analysis of simulations of abnormal grain growth. We found that GB anisotropy introduces a statistical preference for certain grain orientations, leading to changes to the grain size distribution compared to an isotropic system. In our second numerical experiment, we incorporated crystallographic grain boundary energy and examined the evolution of microstructure features at different initial configurations. We observed that the development of texture and the growth of twin grain boundaries were more pronounced when the initial microstructure had a higher fraction of high-angle grain boundaries. These findings suggest effective grain boundary engineering strategies for improving material properties.

In our future work, we aim to enhance the TD method by integrating grain rotation [65] and grain boundary plasticity [66], allowing for the simultaneous evolution of microstructure and deformation. Especially, this is crucial for investigating phenomena such as dynamic recrystallization, superplasticity, and severe plastic deformation [10, 67, 68], which require

a more comprehensive understanding of the underlying mechanisms. We anticipate that incorporating these features will enhance the accuracy and applicability of the model, thereby advancing our ability to predict and optimize material properties.

Declaration of competing interest

The authors declare that they have no known competing financial interests or personal relationships that could have appeared to influence the work reported in this paper.

References

- [1] T. Watanabe, Grain boundary engineering: historical perspective and future prospects, *Journal of Material Science* 46 (2011) 4095–4115.
- [2] K. S. Kumar, H. V. Swygenhoven, S. Suresh, Mechanical behavior of nanocrystalline metals and alloys, *Acta Materialia* 51 (2003) 5743–5774.
- [3] H. A. P. II, B. L. Boyce, A review of fatigue behavior in nanocrystalline metals, *Experimental Mechanics* 50 (2010) 5–23.
- [4] Y. T. Zhu, T. G. Langdon, The fundamentals of nanostructured materials processed by severe plastic deformation, *The Journal of The Minerals, Metals & Materials Society* 56 (2004) 58–63.
- [5] D. B. Bober, M. Kumar, T. J. Rupert, Nanocrystalline grain boundary engineering: Increasing $\Sigma 3$ boundary fraction in pure Ni with thermomechanical treatments, *Acta Materialia* 86 (2015) 43–54.
- [6] G. Palumbo, E. M. Lehigh, P. Lin, Applications for grain boundary engineered materials, *The Journal of The Minerals, Metals & Materials Society* 50 (1998) 40–43.
- [7] T. Frolov, W. Setyawan, R. J. Kurtz, J. Marian, A. R. Oganov, R. E. Rudd, Q. Zhu, Grain boundary phases in bcc metals, *Nanoscale* 10 (2018) 8253–8268.
- [8] K. G. F. Janssens, D. Olmsted, E. A. Holm, S. M. Foiles, S. J. Plimton, P. M. Derlet, Computing the mobility of grain boundaries, *Nature Materials* 5 (2006) 124–127.
- [9] K. D. Molodov, D. A. Molodov, Grain boundary mediated plasticity: On the evaluation of grain boundary migration - shear coupling, *Acta Materialia* 153 (2018) 336–353.
- [10] S. Thomas, K. Chen, J. Han, P. K. Purohit, D. J. Srolovitz, Reconciling grain growth and shear-coupled grain boundary migration, *Nature communications* 8 (2017) 1–12.
- [11] J. Kim, M. Jacobs, S. Osher, N. C. Admal, A crystal symmetry-invariant Kobayashi–Warren–Carter grain boundary model and its implementation using a thresholding algorithm, *Computational Materials Science* 199 (2021) 110575.
- [12] T. Belytschko, R. Gracie, G. Ventura, A review of extended/generalized finite element methods for material modeling, *Modelling and Simulation in Materials Science and Engineering* 17 (2009) 043001.

- [13] Q. Zhao, M. A. Wahab, Y. Ling, Z. Liu, Fatigue crack propagation across grain boundary of Al-Cu-Mg bicrystal based on crystal plasticity XFEM and cohesive zone model, *Journal of Materials Science & Technology* 126 (2022) 275–287.
- [14] W. Liu, Z. He, W. Yao, M. Li, J. Tang, XFEM simulation of the effects of microstructure on the intergranular fracture in high strength aluminum alloy, *Computational Materials Science* 84 (2014) 310–317.
- [15] W. W. Mullins, Two-dimensional motion of idealized grain boundaries, *Journal of Applied Physics* 27 (1956) 900–904.
- [16] K. Barmak, E. Eggeling, D. Kinderlehrer, R. Sharp, S. Ta’asan, A. D. Rollett, K. R. Coffey, Grain growth and the puzzle of its stagnation in thin films: The curious tale of a tail and an ear, *Progress in Materials Science* (2013) 987–1055.
- [17] E. A. Lazar, J. K. Mason, R. D. MacPherson, D. J. Srolovitz, Distribution of topological types in grain-growth microstructures, *Physical Review Letters* 125 (2020) 015501.
- [18] V. Mohles, 3-D front tracking model for interfaces with anisotropic energy, *Computational Materials Science* 176 (2020) 109534.
- [19] H.-K. Kim, S. G. Kim, W. Dong, I. Steinbach, B.-J. Lee, Phase-field modeling for 3d grain growth based on a grain boundary energy database, *Modelling and Simulation in Materials Science and Engineering* 22 (2014) 034004.
- [20] H. Salama, J. Kundin, O. Shchyglo, V. Mohles, K. Marquardt, I. Steinbach, Role of inclination dependence of grain boundary energy on the microstructure evolution during grain growth, *Acta Materialia* 188 (2020) 641–651.
- [21] K. Chen, J. Han, X. Pan, D. J. Srolovitz, The grain boundary mobility tensor, *Proceedings of the National Academy of Sciences of the United States of America* 117 (2020) 4533–4538.
- [22] B. Runnels, I. J. Beyerlein, S. Conti, M. Ortiz, An analytical model of interfacial energy based on a lattice-matching interatomic energy, *Journal of Mechanics and Physics of Solids* 89 (2016) 174–193.
- [23] B. Runnels, I. J. Beyerlein, S. Conti, M. Ortiz, A relaxation method for the energy and morphology of grain boundaries and interfaces, *Journal of Mechanics and Physics of Solids* 94 (2016) 388–408.
- [24] D. L. Olmsted, S. M. Foiles, E. A. Holm, Survey of computed grain boundary properties in face-centered cubic metals: I. grain boundary energy, *Acta Materialia* 57 (2009) 3694–3703.
- [25] H. Hallberg, V. V. Bulatov, Modeling of grain growth under fully anisotropic grain boundary energy, *Modelling and Simulation in Materials Science and Engineering* 27 (2019) 045002.

- [26] S. R. Kalidindi, M. De Graef, Materials Data Science: Current Status and Future Outlook, *Annual Review of Materials Research* 45 (2015) 171–193.
- [27] S. R. Kalidindi, Hierarchical materials informatics: novel analytics for materials data, Elsevier, 2015.
- [28] J. Kim, N. C. Admal, A stochastic framework for evolving grain statistics using a neural network model for grain topology transformations, *Computational Materials Science* 199 (2023) 111812.
- [29] G. Abbruzzese, K. Lücke, A theory of texture controlled grain growth—I. derivation and general discussion of the model, *Acta Metallurgica* 34 (1986) 905–914.
- [30] C. S. Pande, R. A. Masumura, S. P. Marsh, Stochastic analysis of two-dimensional grain growth, *Philosophical Magazine A* 81 (2001) 1229–1239.
- [31] S. Esedoğlu, F. Otto, Threshold dynamics for networks with arbitrary surface tensions, *Communications on Pure and Applied Mathematics* 68 (2015) 808–864.
- [32] E. Eren, B. Runnels, J. Mason, Comparison of evolving interfaces, triple points, and quadruple points for discrete and diffuse interface methods, *Computational Materials Science* 213 (2022) 111632.
- [33] M. Dziwnik, A. Münch, B. Wagner, An anisotropic phase-field model for solid-state dewetting and its sharp-interface limit, *Nonlinearity* 30 (2017) 1465.
- [34] G. Martine, Martine La Boissonière, R. Choksi, K. B. S. Esedoğlu, Statistics of grain growth: Experiment versus the phase-field-crystal and Mullins models, *Materialia* 6 (2019) 100280.
- [35] K. R. Elder, N. Provatas, J. Berry, P. Stefanovic, M. Grant, Phase-field crystal modeling and classical density functional theory of freezing, *Physical Review B* 75 (2007) 064107.
- [36] X. Peng, A. Bhattacharya, S. K. Naghibzadeh, D. Kinderlehrer, R. Suter, K. Dayal, G. S. Rohrer, Comparison of simulated and measured grain volume changes during grain growth, *Physical Review Materials* 6 (2022) 033402.
- [37] J. D. Niño, O. K. Johnson, Influence of grain boundary energy anisotropy on the evolution of grain boundary network structure during 3D anisotropic grain growth, *Computational Materials Science* 217 (2023) 111879.
- [38] V. V. Bulatov, B. W. Reed, M. Kumar, Grain boundary energy function for fcc metals, *Acta Materialia* 65 (2014) 161–175.
- [39] T. Salvador, S. Esedoğlu, A simplified threshold dynamics algorithm for isotropic surface energies, *Journal of Scientific Computing* 79 (2019) 648–669.
- [40] T. Salvador, S. Esedoğlu, The role of surface tension and mobility model in simulations of grain growth, *arXiv:1907.11574* (2019).

- [41] R. Z. Valiev, R. K. Islamgaliev, I. V. Alexandrov, Bulk nanostructured materials from severe plastic deformation, *Progress in Materials Science* 45 (2000) 103–189.
- [42] S. L. Semiatin, A. A. Salem, M. J. Saran, Models for severe plastic deformation by equal-channel angular extrusion, *JOM* 56 (2004) 69–77.
- [43] Y. T. Zhu, T. G. Langdon, The fundamentals of nanostructured materials processed by severe plastic deformation, *JOM* 56 (2004) 58–63.
- [44] J. A. Muñoz, R. E. Bolmaro, A. M. J. Jr, A. Zhilyaev, J. María, Prediction of generation of high- and low-angle grain boundaries (HAGB and LAGB) during severe plastic deformation, *Metallurgical and Materials Transactions A* 51 (2020) 4674–4684.
- [45] B. Merriman, J. K. Bence, S. J. Osher, Diffusion generated motion by mean curvature, *Proceedings of the Computational Crystal Growers Workshop* (1992) 72–83.
- [46] A. Zaitzeff, S. Esedoğlu, K. Garikipati, Second order threshold dynamics schemes for two phase motion by mean curvature, *Journal of Computational Physics* 410 (2020) 109404.
- [47] M. Elsey, S. Esedoğlu, P. Smereka, Diffusion generated motion for grain growth in two and three dimensions, *Journal of Computational Physics* 228 (2009) 8015–8033.
- [48] M. Elsey, S. Esedoğlu, P. Smereka, Large scale simulations and parameter study for a simple recrystallization model, *Philosophical Magazine* 91 (2011) 1607–1642.
- [49] S. E. M. Jacobs, P. Zhang, Kernels with prescribed surface tension & mobility for threshold dynamics schemes, *Journal of Computational Physics* 337 (2017) 62–83.
- [50] C. Herring, *Surface Tension as a Motivation for Sintering*, McGraw Hill, 1951. doi:[10.1007/978-3-642-59938-5_2](https://doi.org/10.1007/978-3-642-59938-5_2).
- [51] H. Ishii, G. E. Pires, P. E. Souganidis, Threshold dynamics type approximation schemes for propagating fronts, *Journal of the Mathematical Society of Japan* 51 (1999) 267–308.
- [52] A. Lawrence, J. M. Rickman, M. P. Harmer, A. D. Rollet, Parsing abnormal grain growth, *Acta Materialia* 103 (2015) 681–687.
- [53] H. V. Atkinson, Overview no. 65: Theories of normal grain growth in pure single phase systems, *Acta Metallurgica* 36 (1988) 469–491.
- [54] W. Mullins, J. Viñals, Linear bubble model of abnormal grain growth, *Acta Materialia* 50 (2002) 2945–2954.
- [55] G. Abbruzzese, K. Lücke, A theory of texture controlled grain growth—i. derivation and general discussion of the model, *Acta Metallurgica* 34 (1986) 905–914.
- [56] E. A. Holm, D. L. Olmsted, S. M. Foiles, Comparing grain boundary energies in face-centered cubic metals: Al, Au, Cu and Ni, *Scripta Materialia* 63 (2010) 905–908.

- [57] V. V. Bulatov, B. W. Reed, M. Kumar, Grain boundary energy function for fcc metals, *Acta Materialia* 65 (2014) 161–175.
- [58] D. Wolf, Structure-energy correlation for grain boundaries in fcc metals—III. Symmetrical tilt boundaries, *Acta Metallurgica et Materialia* 38 (1990) 781–790.
- [59] R. Lapovok, P. F. Thomson, R. Cottam, Y. Estrin, Nanocrystalline grain boundary engineering: Increasing $\Sigma 3$ boundary fraction in pure Ni with thermomechanical treatments, *Acta Materialia* 86 (2015) 43–54.
- [60] M. Dao, L. Lu, Y. F. Shen, S. Suresh, Strength, strain-rate sensitivity and ductility of copper with nanoscale twins, *Acta Materialia* 54 (2006) 5421–5432.
- [61] B. Bay, N. Hansen, D. A. Hughes, D. Kuhlmann-Wilsdorf, Overview no. 96 evolution of f.c.c. deformation structures in polyslip, *Acta Metallurgica et Materialia* 40 (1992) 205–219.
- [62] R. Lapovok, P. F. Thomson, R. Cottam, Y. Estrin, The effect of grain refinement by warm equal channel angular extrusion on room temperature twinning in magnesium alloy ZK60, *Journal of Materials Science* 40 (2005) 1699–1708.
- [63] V. Grand, B. Flipon, A. Gaillac, M. Bernacki, Simulation of continuous dynamic recrystallization using a level-set method, *Materials* 15 (2022) 8547.
- [64] S. Julie, M. K. Dash, N. P. Wasekar, C. David, M. Kamruddin, Effect of annealing and irradiation on the evolution of texture and grain boundary interface in electrodeposited nanocrystalline nickel of varying grain sizes, *Surface & Coatings Technology* 426 (2021) 127770.
- [65] S. Esedoğlu, Grain size distribution under simultaneous grain boundary migration and grain rotation in two dimensions, *Computational Materials Science* 121 (2016) 209–216.
- [66] N. C. Admal, G. Po, J. Marian, A unified framework for polycrystal plasticity with grain boundary evolution, *International Journal of Plasticity* 106 (2018) 1–30.
- [67] C. Wei, L. Zhang, J. Han, D. J. Srolovitz, Y. Xiang, Grain boundary triple junction dynamics: a continuum disconnection model, *SIAM Journal on Applied Mathematics* 80 (2020) 1101–1122.
- [68] B. Runnels, V. Agrawal, Phase field disconnections: A continuum method for disconnection-mediated grain boundary motion, *Scripta Materialia* 186 (2020) 6–10.